RSC Advances

PAPER

View Article Online
View Journal | View Issue

Cite this: *RSC Adv.*, 2023, **13**, 9892

Predicting the speciation of ionizable antibiotic ciprofloxacin by biochars with varying carbonization degrees†

Guowei Shi,[abc] Yasong Li,[ab] Yaci Liu[ab] and Lin Wu *[abd]

Sorption mechanisms of ionizable organic pollutants by biochars and approaches for the prediction of sorption are still unclear. In this study, batch experiments were conducted to explore the sorption mechanisms of woodchip-derived biochars prepared at 200–700 °C (referred as WC200–WC700) for cationic, zwitterionic and anionic species of ciprofloxacin (referred as CIP^+, $CIP^\pm$ and CIP^-, respectively). The results revealed that the sorption affinity of WC200 for different CIP species was in the order of $CIP^\pm$ > CIP^+ > CIP^-, while that of WC300–WC700 remained the order of CIP^+ > $CIP^\pm$ > CIP^-. WC200 exhibited a strong sorption ability, which could be attributed to hydrogen bonding and electrostatic attraction with CIP^+, electrostatic attraction with $CIP^\pm$, and charge-assisted hydrogen bonding with CIP^-. Pore filling and π–π interactions contributed to the sorption of WC300–WC700 for CIP^+, $CIP^\pm$ and CIP^-. Rising temperature facilitated CIP sorption to WC400 as verified by site energy distribution analysis. Proposed models including the proportion of the three CIP species and sorbent aromaticity index (H/C) can quantitatively predict CIP sorption to biochars with varying carbonization degrees. These findings are vital to elucidating the sorption behaviors of ionizable antibiotics to biochars and exploring potential sorbents for environmental remediation.

Received 7th January 2023
Accepted 20th March 2023

DOI: 10.1039/d3ra00122a

rsc.li/rsc-advances

1. Introduction

In recent years, the residue of antibiotics in the aquatic and soil environments has caused many serious environmental problems. As a typical fluoroquinolone antibiotic, ciprofloxacin (CIP) has a wide spectrum of antibacterial properties and is extensively used in disease treatment and livestock breeding.[1] However, most of the CIP is excreted to sewage systems in the form of urine and feces because only a small part of the drugs is absorbed by humans or animals.[2] It was reported that CIP has been detected in water bodies and sediments in several regions of the world.[3,4] For instance, the concentration of CIP in the water body of Firozabad Ditch in Iran reached 656.8 ng L^{-1},[5] and that in the sediment of the Haihe River in China was up to 1290 ng g^{-1}.[6] The heavy use of drugs can cause some problems such as antibiotic abuse and emergence of resistance genes.[7] Due to the existence and potential toxicity of CIP in the environment, it has been regarded as a high-risk pollutant and its pollution control is urgent.[8]

Biochar, as an environment-friendly carbonaceous material with abundant pore structures and surface functional groups, has gradually become a research hotspot.[9,10] The application of biochar in sewage treatment, efficient removal, and functional composite materials has become frontier research topics.[11] It can effectively control the migration of pollutants in soil and groundwater through sorption-locking and display an excellent performance in environmental remediation.[12–14] Certain studies have proven that the addition of hardwood-derived biochars to agricultural soils can reduce the pore water concentration of sulfamethazine and control its migration in soils.[15] In addition, due to strong catalytic properties and compatibility coupled with other materials of biochar, it has been used as a mediator for the degradation of pollutants in sewage treatment. For instance, the higher removal efficiency of oxytetracycline by periodate activated with manganese oxide modified biochar was observed, which provided a promising idea for tackling water pollution.[16] Biochar's applications for global climate mitigation, salinity and drought stress amelioration, and biofuel production are also of great concern.[17]

It has been reported that biochar can effectively sorb CIP and the precursor materials of biochar include rice straw, bagasse, sludge, bamboo, urban solid waste, marine algae, *etc.*[1,18–21] However, report on CIP sorption by biochar derived from

[a]*Fujian Provincial Key Laboratory of Water Cycling and Eco-Geological Processes, Xiamen 361021, China. E-mail: wulin_shs@mail.cgs.gov.cn; Fax: +86-311-67598661; Tel: +86-311-67598598*

[b]*China Geological Survey & Hebei Province Key Laboratory of Groundwater Contamination and Remediation, Institute of Hydrogeology and Environmental Geology, Chinese Academy of Geological Sciences, Shijiazhuang 050061, China*

[c]*China University of Geosciences (Beijing), Beijing 100083, China*

[d]*North China University of Water Resources and Electric Power, Zhengzhou 450046, China*

† Electronic supplementary information (ESI) available. See DOI: https://doi.org/10.1039/d3ra00122a

woodchip, a biomass with high content of lignin and cellulose, is rare. Compared with other plant materials, woody biochars have been of particular interest since the carbon content in woods is retained in a greater percentage.[22] Also, woodchips are common plant waste in nature, with low cost and wide source. Woodchip-derived biochars played an effective role in removing ionizable organic pollutants including tetracycline, levofloxacin, sulfamethazine and ibuprofen,[23–25] which exhibited a broad application prospect in environmental restoration.[26]

Moreover, sorption of ionizable antibiotics was expected to be highly affected by sorbate species and the sorption mechanisms dynamically changed with speciation.[27] For instance, sorption of CIP with different dissociated species by titanate nanotubes was studied through both experimental and theoretical calculations. The results showed that CIP species at various pH exhibited significantly different sorption favorability.[28] Mechanisms relevant to CIP sorption by biochars were summarized based on previous studies, including electrostatic interaction, pore filling, π–π interactions and hydrogen bonding,[19,29] but the effect of speciation on CIP sorption by biochars was still unclear. Also, few models can be used to quantitatively predict the sorption of different CIP species by biochars. Furthermore, previous studies focused on thermodynamic analysis to explore the influence of temperature on sorption, while a deep understanding of site energy distribution of CIP sorption was still lacking.

Therefore, in this study, woodchip-derived biochars were produced by oxygen-limited pyrolysis at 200–700 °C. A series of batch experiments were employed to investigate the sorption behaviors of CIP by biochars. The purposes of this study were to explore the sorption affinity and mechanisms of different CIP species to biochars, and establish a practical model to predict CIP sorption. Furthermore, the effect of temperature on sorption was evaluated by thermodynamics and site energy distribution analysis. This study reveals the speciation and thermodynamic behaviors of CIP sorption by biochars, and provides a novel approach for the sorption prediction of ionizable antibiotics.

2. Materials and methods

2.1 Materials and reagents

Ciprofloxacin (≥98%) was purchased from Shanghai ANPEL Experimental Technology Co., Ltd. It is an amphoteric antibiotic that exhibits cationic, zwitterionic and anionic species of CIP at various pH (Fig. S1†). HCl, NaOH and NaCl (analytically pure) were obtained from Beijing Chemical Works. Acetonitrile (Thermo Fisher Scientific, Shanghai) and potassium dihydrogen phosphate (≥99.5%, Macklin, Shanghai) were chromatographically pure, and deionized water was used in the experiments.

2.2 Preparation and characterization of biochars

Biochars were produced by the oxygen-limited temperature control pyrolysis method. Woodchips were collected from the field of Quanzhou, Fujian Province of China. Firstly, the surface impurities of woodchips were removed by rinsing with water three times, and then dried in a blast drying box at 80 °C for 12 h. Secondly, the pretreated woodchips were sealed in a crucible and placed into a muffle furnace, pyrolyzed at 200, 300, 400, 500, 600, and 700 °C for 6 h, respectively. Finally, the generated biochars were sieved through a 0.3 mm sieve and loaded into a brown bottle for further use. The biochars obtained at 200–700 °C were labeled as WC200–WC700. The temperature range of 200–700 °C was chosen to explore the evolution of sorption mechanisms of biochars with varying carbonization degrees.

Elemental composition (C, H, N) of biochars was determined using the elemental analyzer (Vario EL Cube, Elementar, Germany), and the O content was calculated by mass balance. The surface functional groups were analyzed by Fourier transform infrared spectrometer (iS10 FTIR spectrometer, USA) in the range of 4000–400 cm^{-1} region at 25 °C. The pore size distribution and specific surface area of biochars were measured with the N_2 sorption–desorption method at a relative pressure of 0.99 by a surface area analyzer (Micromeritics ASAP 2460, USA). Surface morphologies of biochars were observed using scanning electron microscopy (SU8020, Hitachi, Japan). Surface charge properties of biochars under different pH conditions were obtained by a zeta potentiometer (Malvern Instruments Ltd, U.K.).

2.3 Batch sorption experiments

Batch experiments were carried out to study the sorption of CIP to biochars. To investigate the effect of pH on sorption, certain dosages of biochars (1 g L^{-1} for WC200 and WC300, 0.5 g L^{-1} for WC400 and WC500, 0.25 g L^{-1} for WC600 and WC700) were weighed in brown glass bottles. Next, 20 mL of CIP solution with the initial concentration of 1, 5, 10, 15, 20, 30 and 40 mg L^{-1} was placed (0.01 mol L^{-1} of NaCl background solution). The initial pH was adjusted to 3.0, 5.8, 7.2, 8.6 and 10.0 with 0.1 M HCl or NaOH according to the proportion of different CIP species. Subsequently, all the samples were kept to the thermostatic shaker with a speed of 175 rpm for 96 h (the equilibrium time obtained from the kinetic experiment) at 298 K. After reaching equilibrium, the samples were centrifuged for 10 min at 3000 rpm and then the supernatants were passed through the membrane (0.45 μm) for analysis. To explore the influence of temperature on sorption, WC200, WC400 and WC600 were selected as representatives of low, medium and high pyrolysis temperature biochars, respectively. The concentration of CIP was repeated as above and the initial solution pH was adjusted to 3.0. The shaker temperatures were controlled at 298 K, 308 K, and 318 K, respectively. All experiments were performed in duplicate and control samples (without biochar) were considered to observe the natural losses (volatilization, degradation and photolysis) of CIP during the experimental process.

CIP concentration was analyzed by high performance liquid chromatography (HPLC, Shimadzu, LC-2030C, Japan) with a Shim-pack GIST C18 column (4.6 mm × 250 mm) at the detection wavelength of 278 nm. The mobile phase A and B were potassium dihydrogen phosphate (0.01 mol L^{-1}, pH was

adjusted to 3.0 with H_3PO_4) and acetonitrile, respectively, with a volume ratio of 77 : 23. The flow rate was 1.0 mL min^{-1} and the injection volume was 10 μL. The retention time was 5 min and the column temperature was 40 °C.

2.4 Data analysis

The Langmuir (eqn (1)) and Freundlich (eqn (2)) models were applied to fit the sorption isotherm data.

$$q_e = \frac{q_m K_L C_e}{K_L C_e + 1} \quad (1)$$

$$q_e = K_F {C_e}^N \quad (2)$$

where C_e is the aqueous-phase concentration at the sorption equilibrium (mg L^{-1}), K_L is the Langmuir sorption constant (L mg^{-1}), K_F is the Freundlich sorption constant ($mg^{(1-N)}$ L^N g^{-1}), q_m is the single-molecule layer sorption capacity (mg g^{-1}), q_e is the equilibrium sorption amount (mg g^{-1}) and N represents the nonlinearity of sorption.

Sorption coefficient K_d (L g^{-1}) was obtained by eqn (3), and energy change and the endothermic or exothermic situation of the sorption process were judged by the thermodynamic models (eqn (4) and (5)):

$$K_d = \frac{q_e}{C_e} \quad (3)$$

$$\Delta G = -RT \ln K_d \quad (4)$$

$$\ln K_d = -\frac{\Delta H}{RT} + \frac{\Delta S}{R} \quad (5)$$

where ΔG denotes Gibbs free energy (kJ mol^{-1}), R is the gas constant (8.314 J mol^{-1} K^{-1}), ΔH represents enthalpy change (J mol^{-1}), ΔS is the entropy change (kJ mol^{-1} K^{-1}) and T is the absolute temperature (K).

Sorption capacity of the heterogeneous surface was obtained by the integral equation as follows:

$$q_e(C_e) = \int_0^{+\infty} q_h(E, C_e) F(E) dE \quad (6)$$

where $q_e(C_e)$ is the maximum sorption capacity (mg g^{-1}), $q_h(E,C_e)$ refers a homogeneous isothermal line on a local sorption site with sorption energy E (kJ mol^{-1}) and $F(E)$ represents energy frequency distribution (mg mol g^{-1} kJ^{-1}).

The relationship between C_e and E^* was described as:

$$C_e = C_s \exp\left(\frac{-E^*}{RT}\right) \quad (7)$$

where C_s was the solubility of solute (mg L^{-1}) and E^* is the sorption energy difference between C_e and C_s (kJ mol^{-1}).

The frequency of site energy distribution $F(E^*)$ was calculated by differentiating $q(E^*)$ to E^*.

$$F(E^*) = -\frac{dq(E^*)}{dE^*} \quad (8)$$

According to the eqn (1), (7) and (8), the generalized Langmuir model (eqn (9)) could be obtained to describe the sorption energy distribution:

$$F(E^*) = \frac{q_m K_L C_s}{RT} \exp\left(\frac{-E^*}{RT}\right) \left[K_L C_s \exp\left(\frac{-E^*}{RT}\right) + 1\right]^{-2} \quad (9)$$

3. Results and discussion

3.1 Properties of woodchip-derived biochars

Pyrolysis temperature is a crucial factor dominating the structures and properties of biochars.[30,31] With the increase of pyrolysis temperature, the content of "black carbon" gradually increased, while the non-carbonated organic matter decreased correspondingly,[32] resulting in the marked increase of carbon content from WC200 to WC700 (49.2% → 87.9%) (Table 1). However, the content of hydrogen and oxygen reduced (5.78% → 1.33% for H and 43.1% → 4.03% for O) owing to the destruction of some surface functional groups at higher temperatures.[33] The element ratios of H/C, O/C and (O + N)/C were reflective of the aromaticity, polarity and hydrophobicity of biochars, respectively.[34] Consequently, the hydrophobicity and aromaticity increased while the polarity decreased from WC200 to WC700.

FTIR spectra of WC200–WC700 was shown in Fig. 1a. The hydroxyl peak was notably weakened from WC200 to WC300 owing to the volatilization of water molecules, and then increasingly disappeared by rising the pyrolysis temperature.[35]

Table 1 The element content and elemental ratio, specific surface area (SSA), total pore volume (V_{total}) and average pore width of woodchip-derived biochars at 200–700 °C (WC200–WC700)

Sample	C (%)	H (%)	O[a] (%)	O/C[b]	H/C[c]	(O + N)/C[d]	SSA (m^2 g^{-1})	V_{total} (cm^3g^{-1})	Average pore width (nm)
WC200	49.2	5.78	43.1	0.658	1.41	0.662	0.920	0.00309	13.4
WC300	68.0	4.83	24.9	0.274	0.853	0.279	1.27	0.00288	9.03
WC400	75.5	3.78	18.1	0.180	0.600	0.184	5.61	0.00620	4.42
WC500	80.0	2.95	12.7	0.119	0.442	0.124	170	0.0954	2.25
WC600	87.9	2.26	4.33	0.0370	0.308	0.0410	367	0.180	1.96
WC700	87.9	1.33	4.03	0.0344	0.182	0.0380	271	0.147	2.17

[a] O content was calculated by mass balance. [b] Atomic ratio of oxygen to carbon. [c] Atomic ratio of hydrogen to carbon. [d] Atomic ratio of oxygen and nitrogen to carbon.

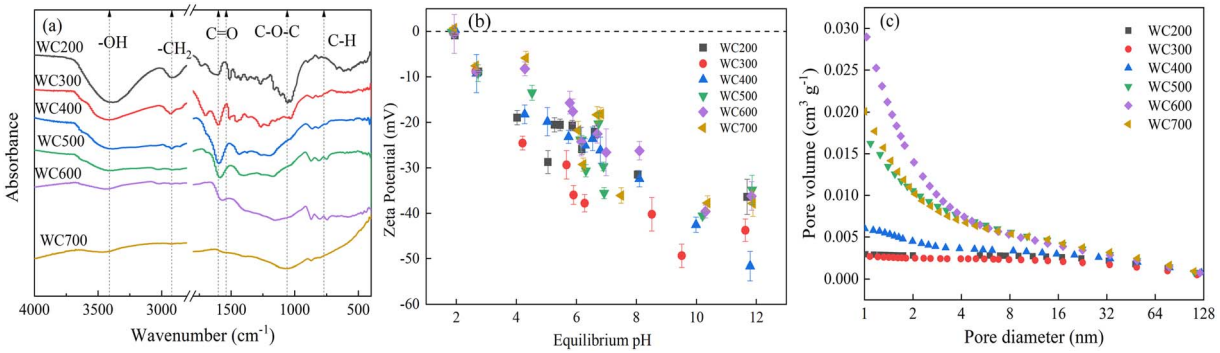

Fig. 1 FTIR spectra (a), zeta potential at different equilibrium pH (b), and pore size distribution (c) of the woodchip-derived biochars at 200–700 °C (WC200–WC700).

Similarly, the $-CH_2$ was gradually reduced and then vanished approximately at 500 °C. Moreover, the sorption peak strength of C=O and C–O–C tended to flatten, while C–H bond peak became significantly stronger, implying an increase in aromaticity. This conclusion fit well with the elemental analysis results. According to Fig. 1b, the pH at the point zero charge (pH_{pzc}) of biochars was estimated to be approximately 2.0. The zeta potential was negative when pH exceeded 2.0 and then gradually decreased as pH increased. Solution pH in this study ranged from 3.0 to 10.0, so the surfaces of the biochars were negatively charged.

The specific surface area (SSA) and pore volume also increased as pyrolysis temperature rose (Fig. 1c and Table 1), which was caused by the release of volatile substances during pyrolysis and the formation of fiber tubular structures with the increase of temperature.[36] The SSA of WC500 suddenly increased by two orders of magnitude (5.61 → 170 $m^2\ g^{-1}$) because the amorphous carbon content decreased and high temperature promoted the formation of holes. The development of pore structure and the formation of micropores caused by high temperature led to a significant increase in SSA.[37] More interestingly, the SSA and pore volume of WC700 were reduced, and the pore size was slightly increased compared with WC600, suggesting that the increasing temperature resulted in the destruction and blockage of some pore structures.[38] Surface morphologies of WC200–WC700 were presented in SEM images (Fig. 2). The surfaces of WC200–WC400 were relatively smooth and the morphological structures were more obvious. The occurrence of micropores was observed on the surface of WC300, but some pores were blocked. When the pyrolysis temperature reached 500 °C, the non-carbonated organic matter was obviously destroyed. As the pyrolysis temperature was beyond 600 °C, biochars were composed of highly concentrated aromatic structures.

3.2 Sorption isotherms of CIP by biochars

Isotherm data was well-fitted to the Langmuir model, depicting that CIP molecules mainly developed a single-molecular layer

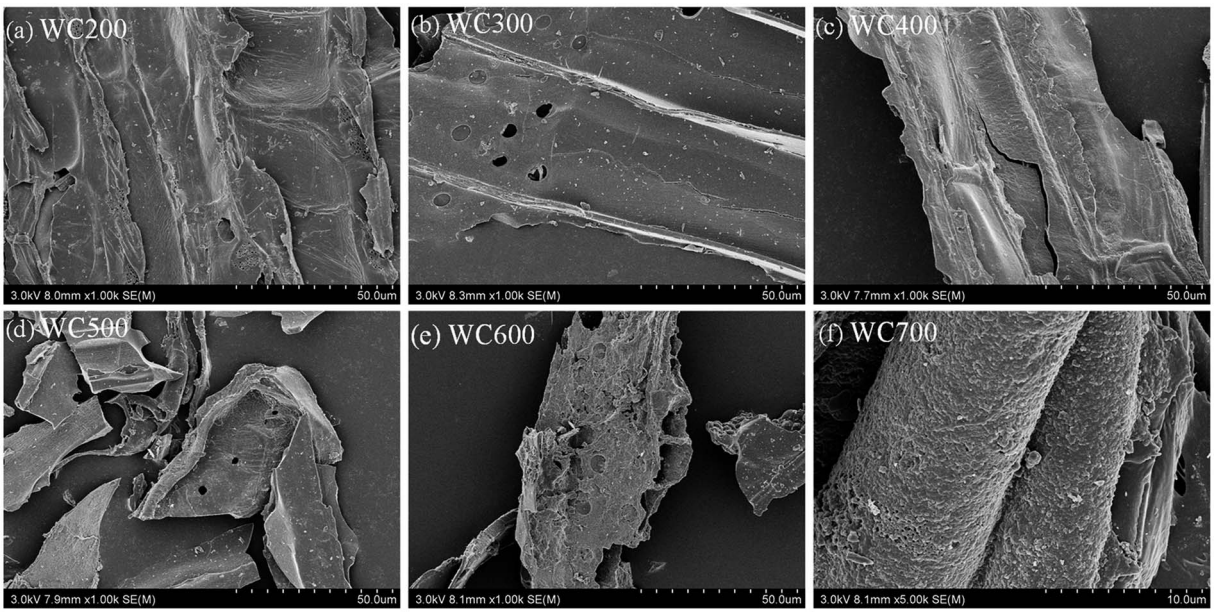

Fig. 2 SEM images of woodchip-derived biochars at 200–700 °C (WC200–WC700).

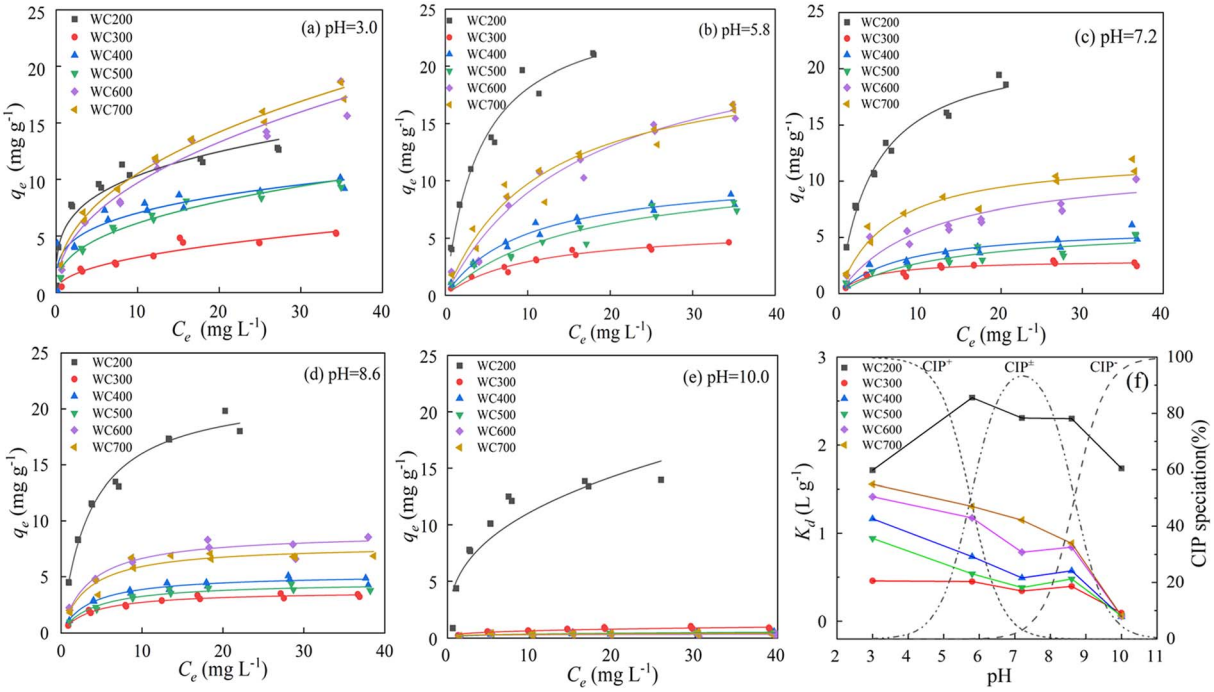

Fig. 3 Sorption isotherms of CIP by woodchip-derived biochars at 200–700 °C (WC200–WC700) under different pH conditions (a–e), sorption coefficient (K_d) of WC200–WC700 and the proportion of different CIP species at various pH (f). The solid lines in panels (a–e) represent the Langmuir model fitting results. K_d was calculated by the ratio of q_e to C_e at C_e = 5 mg L^{-1}.

coverage on the biochar surfaces.[21] The CIP–biochar sorption isotherms under certain pH conditions were presented in Fig. 3a–e, and the fitting parameters were summarized in Table 2. The maximum sorption amount of 21.15 mg g^{-1} was observed for WC200 at pH 5.8. Sorption affinity of the woodchip-derived biochars at 200–700 °C displayed a similar tendency that a gradual increase in q_e was exhibited as C_e increased. Pyrolysis temperature was the main factor governing sorption capacity. The K_d values of biochars were ranked as WC200 > WC700 > WC600 > WC400 > WC500 > WC300 (Fig. 3f). WC200 exhibited a strong sorption performance compared to the high-temperature biochars. This conclusion was similar to the previous study that the sorption capacity of 250 °C biochar for sulfamethoxazole was higher than high-temperature biochars.[39]

The pH of solution has a crucial impact on the sorption process of ionic organic pollutants.[40,41] For WC300–WC700, the values of K_d were negatively correlated with pH and the variation of that showed a similar trend (Fig. 3f). Specifically, the K_d values decreased significantly with the increase in pH from 3.0 to 7.2. At pH 7.2–8.6, the K_d values of WC300–WC600 increased slightly and that of WC700 still decreased. When pH rose above 8.6, the sorption was apparently affected by pH and the sorption capacity decreased drastically. In contrast with WC300–WC700, the increased solution pH resulted in the increased and then decreased sorption capacity of WC200. WC200 displayed an excellent sorption performance under near-neutral conditions (5.8 < pH < 8.6). The results demonstrated that the sorption of WC200 for different CIP species ranked as CIP$^\pm$ > CIP$^+$ > CIP$^-$, while that of WC300–WC700 was in the order of CIP$^+$ > CIP$^\pm$ > CIP$^-$.

3.3 Dynamic changes in sorption mechanisms

Properties of biochar have a great influence on sorption mechanism. To identify the effect of SSA and oxygen content on sorption, SSA-normalized and oxygen content-normalized sorption isotherms were investigated (Fig. 4). SAA-normalized K_F ($K_{F\text{-}SAA}$) of WC200 was significantly greater than other biochars (Table 2), indicating that polarity had a great contribution to its sorption. This result was comparable to the previous research that the sorption capacity per unit SSA of 300 °C biochar for *N*-acyl homoserine lactones was higher than that of 600 °C biochar.[42] A previous study showed that some oxygen-containing groups on the biochar surfaces such as –COOH and –OH could become the main hydrogen-bonding sorption positions for ionic organic pollutants.[43] Based on the elemental and FTIR analysis, WC200 had the highest H and O content and the –OH stretching vibration peak was the most intense. These oxygen-containing groups promoted sorption by acting with polar functional groups such as –COOH on CIP through hydrogen bonding. Moreover, the electrostatic attraction between CIP and WC200 was strong due to more negatively charged functional groups of WC200. Thus, polarity dominated the sorption of CIP to WC200 through electrostatic attraction and hydrogen bonding.

In addition, the oxygen content-normalized K_F ($K_{F\text{-}O}$) values of WC600 and WC700 were apparently higher than low-temperature biochars, which meant that high-temperature

Table 2 Sorption isothermal model parameters of the woodchip-derived biochars at 200–700 °C (WC200–WC700) for CIP under different pH values

		Langmuir			Freundlich				
pH	Sample	q_m (mg g^{-1})	K_L (L mg^{-1})	R^2	K_F (mg$^{(1-N)}$ L^N g^{-1})	$K_{F\text{-}SSA}$[a] (mg$^{(1-N)}$ L^N m^{-2})	$K_{F\text{-}O}$[b] (mg$^{(1-N)}$ L^N g^{-1})	N	R^2
3.0	WC200	12.2	1.03	0.958	5.55	2.53	0.0539	0.270	0.911
	WC300	6.46	0.109	0.941	1.12	0.877	0.0450	0.446	0.927
	WC400	10.1	0.316	0.813	3.74	0.411	0.128	0.275	0.835
	WC500	11.0	0.156	0.983	2.53	0.0149	0.199	0.386	0.961
	WC600	19.6	0.093	0.950	3.40	0.00927	0.786	0.455	0.957
	WC700	21.6	0.107	0.971	3.88	0.0143	0.962	0.433	0.988
5.8	WC200	25.7	0.236	0.974	6.35	6.91	0.147	0.431	0.955
	WC300	5.13	0.165	0.812	0.993	0.956	0.0490	0.447	0.859
	WC400	10.7	0.102	0.977	1.77	0.316	0.0979	0.452	0.952
	WC500	12.6	0.046	0.864	1.27	0.00649	0.0870	0.519	0.893
	WC600	23.9	0.060	0.951	2.46	0.00669	0.567	0.542	0.933
	WC700	20.8	0.088	0.948	3.01	0.0111	0.746	0.481	0.944
7.2	WC200	22.2	0.231	0.981	5.64	6.14	0.131	0.409	0.966
	WC300	3.02	0.264	0.911	0.967	1.05	0.0389	0.311	0.843
	WC400	6.01	0.127	0.876	1.19	0.212	0.0660	0.418	0.904
	WC500	6.01	0.083	0.822	0.912	0.00536	0.0719	0.458	0.885
	WC600	11.7	0.090	0.851	1.91	0.00521	0.442	0.444	0.923
	WC700	12.3	0.164	0.916	2.74	0.0100	0.679	0.397	0.925
8.6	WC200	21.8	0.277	0.980	6.28	6.83	0.136	0.376	0.948
	WC300	3.73	0.266	0.970	1.21	0.950	0.0487	0.306	0.878
	WC400	5.24	0.280	0.960	1.79	0.319	0.0990	0.292	0.853
	WC500	4.53	0.252	0.947	1.50	0.00881	0.118	0.294	0.816
	WC600	8.96	0.286	0.943	3.04	0.00827	0.701	0.291	0.863
	WC700	8.01	0.313	0.822	2.82	0.0104	0.698	0.268	0.773
10	WC200	16.3	0.312	0.965	4.87	5.29	0.113	0.358	0.842
	WC300	1.07	0.199	0.993	0.236	0.249	0.0128	0.424	0.894
	WC400	0.583	0.200	0.965	0.132	0.0295	0.00916	0.417	0.840
	WC500	0.314	0.507	0.858	0.185	0.00109	0.0146	0.279	0.798
	WC600	0.592	0.193	0.806	0.152	0.000630	0.0534	0.397	0.357
	WC700	0.798	0.159	0.928	0.119	0.000822	0.0554	0.571	0.879

[a] Specific surface area normalized Freundlich sorption constant. [b] Oxygen content normalized Freundlich sorption constant.

biochars had higher aromaticity and then provided more π–π interaction sites.[44] For example, the benzene rings of CIP could become electron receptors on account of the strong electron attraction of F atoms, while some aromatic structures on the surfaces of biochars can be used as electron donors. Thus, sorption was promoted by π–π interactions. Moreover, high-temperature biochars contained larger SSA and abundant pore structures which provided more sorption sites and CIP could be adsorbed to biochars through pore-filling.[35]

For WC300–WC700, they exhibited higher sorption for CIP^+ than $CIP^\pm$ and CIP^- owing to the electrostatic attraction between the negatively charged biochars and CIP^+. As pH increased, –COOH gradually dissociated and the proportion of $CIP^\pm$ increased, causing the weakening of electrostatic attraction. It was worth noting that the sorption changed slightly as pH rose from 7.2 to 8.6, indicating the effect of electrostatic interactions on $CIP^\pm$ sorption was small. When pH exceeded 8.6, CIP^- became the main form of CIP in the solution and the sorption was hindered due to the strong electrostatic repulsion. Similarly, titanate nanotubes showed higher sorption for CIP^+ than $CIP^\pm$ and CIP^-, which could result from the transition from electrostatic attraction to repulsion.[28]

The sorption capacity of WC200 for CIP increased rapidly over the pH range of 3.0 to 5.8. It was because CIP had smaller solubility and stronger hydrophobicity as pH increased, resulting in more sorption of CIP molecules to the surfaces of WC200 through electrostatic attraction and hydrogen bonding. Furthermore, the result showed the optimal sorption capacity and less variation at pH 5.8–8.6, illustrating the sorption was insensitive to this pH range while $CIP^\pm$ was dominant. When pH exceeded 8.6, a gradual decrease in sorption was attributed to the strong electrostatic repulsion and the weakening of the hydrophobic effect. Notably, WC200 still maintained a certain sorption amount for CIP^- compared with other biochars (Fig. 4f), which could be associated with the formation of negative charge-assisted hydrogen bonding (–CAHB). Specifically, neutral CIP was released because CIP^- captured H^+ in water molecules, and then hydrogen bonding was formed between neutral CIP and WC200. The hypothesis was similar to the formation of –CAHB on sulfonamides sorption under alkaline conditions.[39,40] Specifically, the proposed possible sorption mechanisms of CIP^+, $CIP^\pm$ and CIP^- by woodchip-derived biochars were exhibited in Fig. 5.

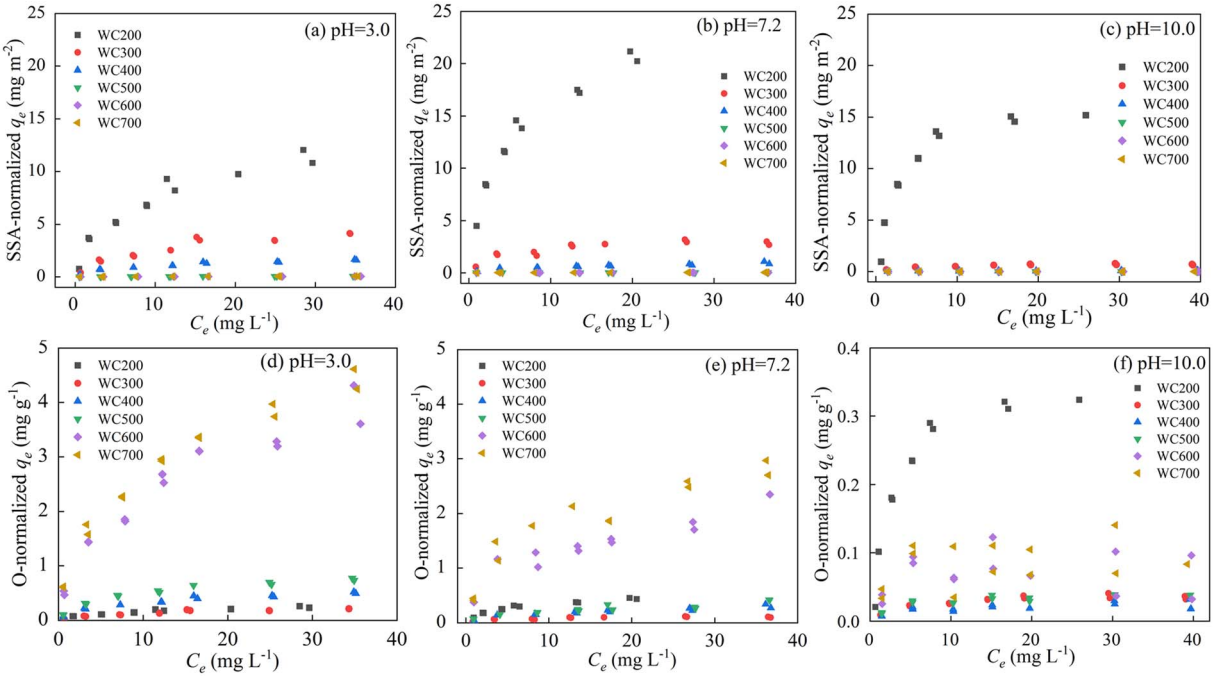

Fig. 4 Specific surface area (SSA)-normalized (a–c) and oxygen content-normalized (d–f) sorption isotherms of woodchip-derived biochars at 200–700 °C (WC200–WC700) for CIP under different pH conditions. The pH was adjusted to 3.0, 7.2 and 10.0 to make cationic CIP, zwitterionic CIP and anionic CIP dominant in the solution, respectively.

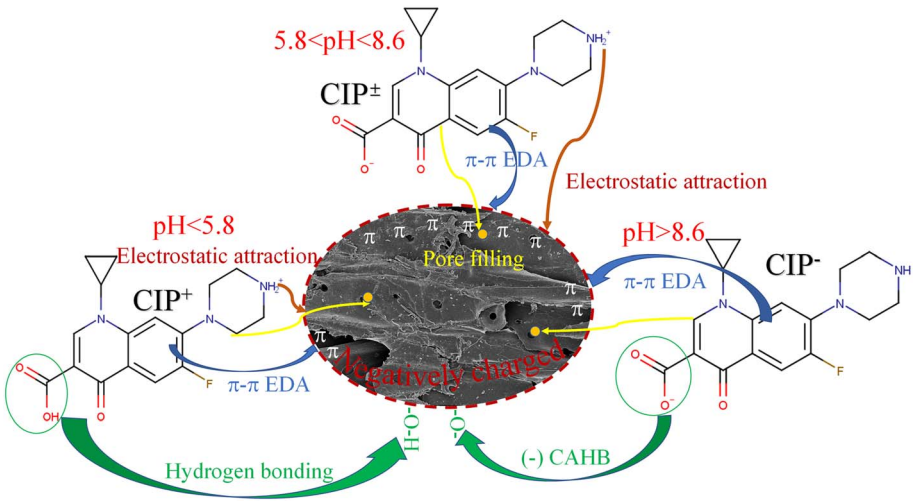

Fig. 5 Proposed possible sorption mechanisms of cationic CIP (CIP^+), zwitterionic CIP ($CIP^{\pm}$) and anionic CIP (CIP^-) by woodchip-derived biochars under varied pH conditions.

3.4 Thermodynamics and site energy distribution

According to Fig. S2 and Table S1,† the sorption increased to varied degrees with the rise of the reaction temperature. This meant that more CIP molecules diffused onto the surfaces of biochars at higher temperatures. Usually, the viscosity of water gradually reduced as temperature rose, causing the decrease of the resistance on solid–liquid boundary layer. Specifically, the effects of temperature on the sorption of WC400 and WC600 were more obvious than WC200. This difference could be explained that the pores of the medium–high temperature biochars were gradually exposed and the biochar surfaces were activated with increasing temperature.[45] It was assumed that pore filling was more sensitive to temperature than hydrogen bonding. According to Table S2,† all the values of ΔG were negative (−2.31 to −0.38 kJ mol^{-1}), indicating that CIP sorption was spontaneous and thermodynamics favorable. This was in accordance with a previously reported result about CIP sorption.[46] The positive value of ΔH (4.54–20.9 kJ mol^{-1}) showed that CIP sorption to biochar was an endothermic process.

Moreover, a gradual increase in sorption randomness was further proved by the positive values of ΔS (0.019–0.074 kJ mol^{-1} K^{-1}).

According to Fig. 6a–c, the value of site energy E^* *versus* CIP loading for three kinds of biochars presented a similar trend. With the increase in CIP loading, E^* acutely decreased, indicating that CIP preferentially took up the high-energy sorption points, and then moved to the low-energy sorption sites on biochars. The results were similar to the energy change of tetracycline sorption to biochars.[47] The curves of site energy distribution for CIP sorption also exhibited similar features (Fig. 6d–f). With the increase in sorption energy, $F(E^*)$ increased to achieve a peak, and then dramatically decreased in the range of experimental data. The peak value of curve ($F(E^*)$) represented the maximum distribution frequency at the specific site energy referred as E_0^* and the area below the curve could be deemed to be the number of sorption sites.[48,49] It was observed that the area under the curve of WC400 gradually enlarged with increasing temperature. This phenomenon could be interpreted that more high-energy sorption sites were obtained at higher temperatures, which promoted the sorption affinity between CIP and biochar. Furthermore, WC600 exhibited a higher $F(E^*)$ value compared with WC200 and WC400, suggesting there were more high-energy sites for CIP sorption to WC600.

Moreover, the right side of E_0^* in the energy distribution was defined as the high-energy area and the left side was the low-energy area.[50] Therefore, CIP sorption was concentrated on low-energy and middle-energy site areas according to Fig. 6d–f. Noticeably, E_0^* of WC600 increased when temperature rose from 298 K to 308 K, which could be due to the enhancement of π–π interactions. It could be elucidated that increasing temperature made π-acceptors and π-donors of biochar surfaces more activated, causing a slight reinforcement of sorption.[47] Less movement of E_0^* in energy distribution curve of WC200 resulted from the insensitivity of hydrogen bonding to temperature, which was consistent with the results of thermodynamic studies. As for WC400, although E_0^* changed slightly, the increase in $F(E^*)$ value could be due to the exposure of the sorption sites as temperature increased.

3.5 Prediction of CIP sorption to biochars

Due to the different sorption behaviors of CIP species to biochars, two improved Freundlich models were proposed to predict CIP sorption affected by speciation. H/C, O/H and SSA, representing the aromaticity, polarity and specific surface area of biochars, respectively, were considered as the important parameters affecting sorption.[51] For WC300–WC700, H/C showed a preferable linear relationship with K_F and N from Freundlich model compared with SSA and O/C, thus it was chosen as the sorbent parameter to predict sorption. The improved Freundlich model was proposed as:

$$q_e = (aH/C + b)C_e^{(cH/C+d)} \quad (10)$$

where H/C represents the aromaticity of biochar, and a, b, c and d are the model fitting parameters.

The speciation model could be described as:[52,53]

$$K_d = K_d^+\alpha^+ + K_d^\pm\alpha^\pm + K_d^-\alpha^- \quad (11)$$

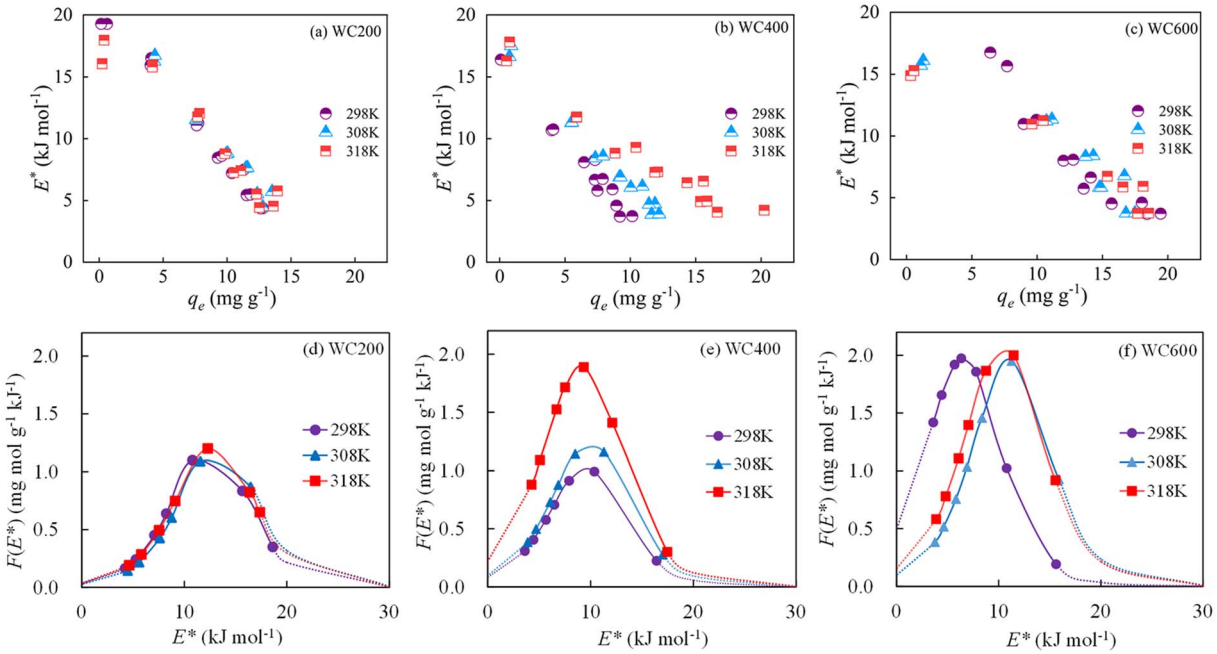

Fig. 6 Site energy (E^*) against CIP loading (a–c) and the site energy distribution of CIP sorption (d–f) by woodchip-derived biochars at 200 °C (WC200), 400 °C (WC400) and 600 °C (WC600) at different temperatures (298 K, 308 K and 318 K). In curves (d–f), the data within the experimental scope on site energy distribution are represented by solid lines, and the data outside the experimental scope on that are denoted by the dotted lines.

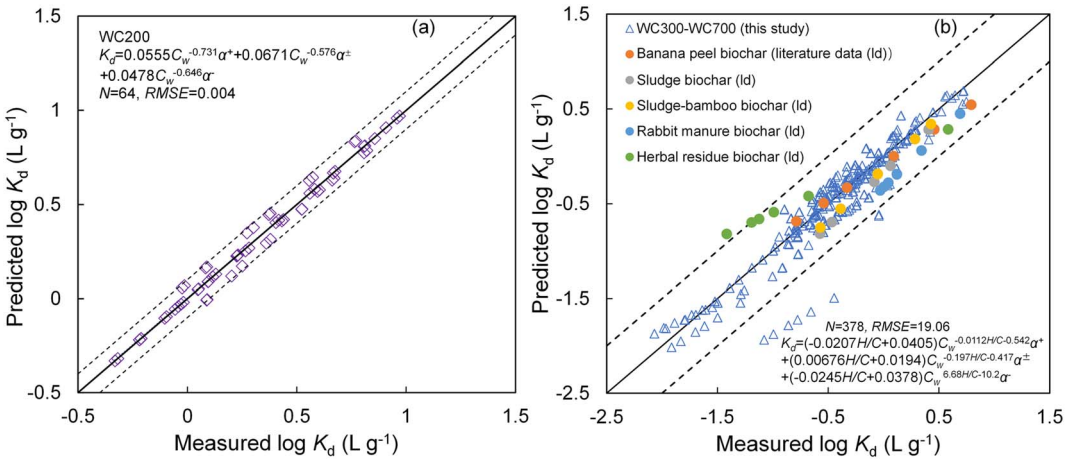

Fig. 7 Modeled and measured log K_d values of CIP to woodchip-derived biochar at 200 °C (WC200) (a) and comparison between the measured and modeled log K_d values of CIP to woodchip-derived biochars at 300–700 °C (WC300–WC700) and other biochars reported in literature: banana peel-derived biochar at 750 °C,[54] sludge and sludge-bamboo derived biochars at 700 °C,[19] rabbit manure biochar at 400 °C,[55] and herbal residue-derived biochar at 800 °C (b).[56] The 1 : 1 line is represented by the solid lines, and 0.2 (a) and 0.5 (b) log unit deviations are represented by the dotted lines. *H*/*C* indicates the aromaticity of biochars, and α^+, $\alpha^\pm$ and α^- indicates the percentage of CIP$^+$, CIP$^\pm$ and CIP$^-$ in solution, respectively (%). *N* represents the number of fitting points. RMSE denotes the root mean squared error.

where K_d^+, $K_d^\pm$ and K_d^- are the sorption coefficient of cationic, zwitterionic and anionic species of CIP, respectively, and α^+, $\alpha^\pm$ and α^- are their percentage in the solution (%), respectively.

According to the eqn (10), (11) and (3), two modified Freundlich models (eqn (12) and (13)) could be obtained to predict CIP sorption.

$$K_d = K_F^+ C_w^{N^+-1}\alpha^+ + K_F^\pm C_w^{N\pm-1}\alpha^\pm + K_F^- C_w^{N^--1}\alpha^- \quad (12)$$

$$K_d = (a_1 H/C + b_1)C_w^{(c_1 H/C+d_1)}\alpha^+ + (a_2 H/C + b_2)C_w^{(c_2 H/C+d_2)}\alpha^\pm + (a_3 H/C + b_3)C_w^{(c_3 H/C+d_3)}\alpha^- \quad (13)$$

where K_F^+, N^+, $K_F^\pm$, $N^\pm$, K_F^- and N^- are the model fitting parameters for WC200, and a_1–a_3, b_1–b_3, c_1–c_3 and d_1–d_3 are the model fitting parameters for WC300–WC700.

The proposed model parameters were calculated by Microsoft Excel solver tool according to the experiment data on CIP sorption and then the predicted log K_d values of CIP to WC200 and WC300–WC700 were obtained from eqn (12) and (13), respectively.

The prediction models performed excellently in depicting the sorption for different species of CIP by biochars (Fig. 7a and b). Specifically, most deviations between the modeled and measured K_d values of CIP to WC200 and WC300–WC700 were less than 0.2 and 0.5 log unit, respectively. However, some modeled K_d values of CIP$^-$ to WC300–WC700 were lower than experimental values in this study, with deviations more than 0.5 log unit. It was speculated that this underestimation may be due to the strong electrostatic repulsion between CIP$^-$ and biochars. Furthermore, some data regarding CIP sorption reported in other literature were collected to verify the practicality of the model,[19,54–56] and the results showed that the prediction effect was good, with deviations between measured and modeled K_d values within 0.5 log unit (Fig. 7b). These deviations may be ascribed to the pH change during the sorption process, causing the slight change of the proportion of different CIP species in the solution. Overall, the deviations between the measured and modeled values of K_d for all the data were less than 1 log unit. The established models can be well applied to predict the sorption of ionizable antibiotic CIP to biochars.

It is noting that the models are more suitable for application in water environment, which can quantitatively predict the sorption behavior of CIP at the biochar–water interface. When biochar is added to the soil, the soil may cause changes in the physical and chemical properties of biochars by clogging the pores of biochars.[57] This will affect the sorption prediction accuracy. Thus, it is necessary to further analyze the influence of actual environmental conditions, such as soil components and its inherent properties, on sorption and continuously improve the accuracy of the prediction mode.

4. Conclusions

Sorption mechanisms dynamically changed with pyrolysis temperature of biochar and CIP speciation. Sorption affinity of WC200 for different forms of CIP decreased as CIP$^\pm$ > CIP$^+$ > CIP$^-$, while that of WC300–WC700 followed the order of CIP$^+$ > CIP$^\pm$ > CIP$^-$. Sorption thermodynamics implied that the sorption process was spontaneous and endothermic. The analysis of site energy distribution suggested that rising temperature caused the increase in the site energy and its maximum occurring frequency, leading to the marked enhancement of CIP sorption by WC400. It can be speculated that high-temperature biochars (WC600 or WC700) could be appropriately amended to strongly acidic water environment to immobilize CIP owing to their higher sorption for CIP$^+$ at pH 3.0, while WC200 could be used to remove CIP at a wider pH range. Sorption of CIP to WC200–WC700 and other kinds of biochars with varying carbonization degrees could be well predicted by

the proposed models regarding sorbate speciation and sorbent aromaticity, with most deviations of sorption coefficient (K_d) within 0.5 log unit. These findings revealed the difference in sorption mechanism of biochars with varying carbonization degrees for ionizable antibiotics.

Author contributions

Guowei Shi: formal analysis, investigation, visualization, writing – original draft. Yasong Li: conceptualization, methodology, resources, validation. Yaci Liu: data curation, writing – review & editing. Lin Wu: funding acquisition, project administration, supervision.

Conflicts of interest

We declare that we have no conflicts of interest to this work.

Acknowledgements

This work was funded by the National Natural Science Foundation of China (41902259), the Natural Science Foundation of Hebei Province of China (D2020504006) and China Geological Survey project (DD20190303).

References

1 T. B. Nguyen, Q. M. Truong, C. W. Chen, W. H. Chen and C. D. Dong, *Bioresour. Technol.*, 2022, **351**, 127043.
2 Q. Sun, M. Li, C. Ma, X. Chen, X. Xie and C. Yu, *Environ. Pollut.*, 2016, **208**, 371–381.
3 H. Zhang, Y. Zhou, Y. Huang, L. Wu, X. Liu and Y. Luo, *Chemosphere*, 2016, **152**, 229–237.
4 N. Gottschall, E. Topp, C. Metcalfe, M. Edwards, M. Payne, S. Kleywegt, P. Russell and D. R. Lapen, *Chemosphere*, 2012, **87**, 194–203.
5 R. Mirzaei, M. Yunesian, S. Nasseri, M. Gholami, E. Jalilzadeh, S. Shoeibi and A. Mesdaghinia, *Sci. Total Environ.*, 2018, **619**, 446–459.
6 L. Zhou, G. Ying, J. Zhao, J. Yang, L. Wang, B. Yang and S. Liu, *Environ. Pollut.*, 2011, **159**, 1877–1885.
7 S. M. Zainab, M. Junaid, N. Xu and R. N. Malik, *Water Res.*, 2020, **187**, 116455.
8 S. Ganesan, M. Amirthalingam, P. Arivalagan, S. Govindan, S. Palanisamy, A. P. Lingassamy and V. K. Ponnusamy, *J. Environ. Manage.*, 2019, **245**, 409–417.
9 A. N. Ngigi, Y. S. Ok and S. Thiele-Bruhn, *J. Hazard. Mater.*, 2019, **364**, 663–670.
10 B. Zhao, H. Xu, F. Ma, T. Zhang and X. Nan, *RSC Adv.*, 2019, **9**, 5218–5223.
11 F. Qin, J. Li, C. Zhang, G. Zeng, D. Huang, X. Tan, D. Qin and H. Tan, *Sci. Total Environ.*, 2022, **818**, 151774.
12 F. Lian and B. Xing, *Environ. Sci. Technol.*, 2017, **51**, 13517–13532.
13 A. Zielińska and P. Oleszczuk, *Environ. Sci. Pollut. Res.*, 2016, **23**, 21822–21832.
14 Y. Sun, T. Wang, L. Bai, C. Han and X. Sun, *J. Environ. Chem. Eng.*, 2022, **10**, 108292.
15 M. Teixido, C. Hurtado, J. J. Pignatello, J. L. Beltran, M. Granados and J. Peccia, *Environ. Sci. Technol.*, 2013, **47**, 6197–6205.
16 G. Fang, J. Li, C. Zhang, F. Qin, H. Luo, C. Huang, D. Qin and Z. Ouyang, *Environ. Pollut.*, 2022, **300**, 118939.
17 P. Wu, B. P. Singh, H. Wang, Z. Jia, Y. Wang and W. Chen, *Biochar*, 2023, **5**, 6.
18 X. Zheng, X. He, H. Peng, J. Wen and S. Lv, *Bioresour. Technol.*, 2021, **334**, 125238.
19 J. Li, G. Yu, L. Pan, C. Li, F. You and Y. Wang, *Environ. Sci. Pollut. Res.*, 2020, **27**, 22806–22817.
20 K. Luo, Y. Pang, Q. Yang, D. Wang, X. Li, L. Wang, M. Lei and J. Liu, *Chemosphere*, 2019, **231**, 495–501.
21 Y. Ma, M. Li, P. Li, L. Yang, L. Wu, F. Gao, X. Qi and Z. Zhang, *Bioresour. Technol.*, 2021, **319**, 10.
22 N. Boraah, S. Chakma and P. Kaushal, *J. Environ. Chem. Eng.*, 2022, **10**, 107825.
23 S. Z. Yi, B. Gao, Y. Y. Sun, J. C. Wu, X. Q. Shi, B. J. Wu and X. Hu, *Chemosphere*, 2016, **150**, 694–701.
24 P. Liu, W. Liu, H. Jiang, J. Chen, W. Li and H. Yu, *Bioresour. Technol.*, 2012, **121**, 235–240.
25 L. Li, D. Zou, Z. Xiao, X. Zeng, L. Zhang, L. Jiang, A. Wang, D. Ge, G. Zhang and F. Liu, *J. Cleaner Prod.*, 2019, **210**, 1324–1342.
26 X. Zhou, L. Shi, T. B. Moghaddam, M. Chen, S. Wu and X. Yuan, *J. Hazard. Mater.*, 2022, **425**, 128003.
27 M. B. Ahmed, J. L. Zhou, H. H. Ngo, W. Guo, M. A. H. Johir and K. Sornalingam, *Chem. Eng. J.*, 2017, **311**, 348–358.
28 H. Ji, T. Wang, T. Huang, B. Lai and W. Liu, *J. Cleaner Prod.*, 2021, **278**, 123924.
29 T.-B. Nguyen, Q.-M. Truong, C.-W. Chen, W.-H. Chen and C.-D. Dong, *Bioresour. Technol.*, 2022, **351**, 127043.
30 J. A. Ippolito, L. Cui, C. Kammann, N. Wrage-Mönnig, J. M. Estavillo, T. Fuertes-Mendizabal, M. L. Cayuela, G. Sigua, J. Novak, K. Spokas and N. Borchard, *Biochar*, 2020, **2**, 421–438.
31 J. Z. Lima, A. P. Ogura, L. C. M. d. Silva, I. M. R. Nauerth, V. G. S. Rodrigues, E. L. G. Espíndola and J. P. Marques, *J. Environ. Chem. Eng.*, 2022, **10**, 108192.
32 G. Sigmund, H. Sun, T. Hofmann and M. Kah, *Environ. Sci. Technol.*, 2016, **50**, 3641–3648.
33 X. Fan, X. Wang, B. Zhao, J. Wan, J. Tang and X. Guo, *J. Environ. Chem. Eng.*, 2022, **10**, 107328.
34 Q. Fang, B. Chen, Y. Lin and Y. Guan, *Environ. Sci. Technol.*, 2014, **48**, 279–288.
35 M. Ahmad, S. S. Lee, A. U. Rajapaksha, M. Vithanage, M. Zhang, J. S. Cho, S. E. Lee and Y. S. Ok, *Bioresour. Technol.*, 2013, **143**, 615–622.
36 X. Tan, Y. Liu, G. Zeng, X. Wang, X. Hu, Y. Gu and Z. Yang, *Chemosphere*, 2015, **125**, 70–85.
37 Y. Sun, G. Yang, L. Zhang and Z. Sun, *Process Saf. Environ. Prot.*, 2017, **107**, 281–288.
38 K. Weber and P. Quicker, *Fuel*, 2018, **217**, 240–261.
39 F. Lian, B. Sun, Z. Song, L. Zhu, X. Qi and B. Xing, *Chem. Eng. J.*, 2014, **248**, 128–134.

40 C. Peiris, S. R. Gunatilake, T. E. Mlsna, D. Mohan and M. Vithanage, *Bioresour. Technol.*, 2017, **246**, 150–159.
41 M. Kah, G. Sigmund, F. Xiao and T. Hofmann, *Water Res.*, 2017, **124**, 673–692.
42 H. Sheng, Y. Yin, L. Xiang, Z. Wang, J. D. Harindintwali, J. Cheng, J. Ge, L. Zhang, X. Jiang, X. Yu and F. Wang, *Chemosphere*, 2022, **299**, 134446.
43 J. Ni, J. J. Pignatello and B. Xing, *Environ. Sci. Technol.*, 2011, **45**, 9240–9248.
44 F. Xiao and J. J. Pignatello, *Water Res.*, 2015, **80**, 179–188.
45 R. Han, W. Zou, H. Li, Y. Li and J. Shi, *J. Hazard. Mater.*, 2006, **137**, 934–942.
46 J. Zhao, G. Liang, X. Zhang, X. Cai, R. Li, X. Xie and Z. Wang, *Sci. Total Environ.*, 2019, **688**, 1205–1215.
47 Y. Zhou, Y. He, Y. He, X. Liu, B. Xu, J. Yu, C. Dai, A. Huang, Y. Pang and L. Luo, *Sci. Total Environ.*, 2019, **650**, 2260–2266.
48 J. Liu, B. Zhou, H. Zhang, J. Ma, B. Mu and W. Zhang, *Bioresour. Technol.*, 2019, **294**, 122152.
49 X. Shen, X. Guo, M. Zhang, S. Tao and X. Wang, *Environ. Sci. Technol.*, 2015, **49**, 4894–4902.
50 X. Li, F. Lei, B. Li and E. Bi, *J. Environ. Qual.*, 2021, **50**, 706–716.
51 G. Sigmund, M. Gharasoo, T. Hüffer and T. Hofmann, *Environ. Sci. Technol.*, 2020, **54**, 4583–4591.
52 Z. Chen, X. Xiao, B. Xing and B. Chen, *Environ. Pollut.*, 2019, **248**, 48–56.
53 M. Teixidó, J. J. Pignatello, J. L. Beltrán, M. Granados and J. Peccia, *Environ. Sci. Technol.*, 2011, **45**, 10020–10027.
54 M. Patel, R. Kumar, C. U. Pittman and D. Mohan, *Environ. Res.*, 2021, **201**, 111218.
55 W. Huang, J. Chen and J. Zhang, *Environ. Technol.*, 2020, **41**, 1380–1390.
56 J. Shang, X. Kong, L. He, W. Li and Q. Liao, *Int. J. Environ. Sci. Technol.*, 2016, **13**, 2449–2458.
57 Y. Liu and J. Chen, *Chemosphere*, 2022, **292**, 133427.